# Design Options for Hybrid Trains Powered by Hydrogen Fuel Cells and Batteries for Routes in the Highlands of Scotland.

## Results for the case of a three-coach multiple-unit train.

### A Report for the Scottish Association for Public Transport

David Murray-Smith

Honorary Senior Research Fellow
and Emeritus Professor of Engineering Systems and Control,
James Watt School of Engineering, University of Glasgow

**Email:** David.Murray-Smith@glasgow.ac.uk

27th August 2020

**Abstract:** This work builds on and extends a report prepared for the Scottish Association for Public Transport in June 2020 entitled *Modelling and simulation of hybrid electric trains powered by hydrogen fuel cells and batteries for routes in the highlands of Scotland*: *Preliminary results*. That report discussed some issues arising in the design of powertrain systems for hybrid hydrogen fuel-cell/battery-electric trains and included preliminary simulation results for the case of a two-coach multiple-unit train.

The choice of power ratings of hydrogen fuel cell stacks and battery packs, along with battery storage capacity in fuel cell/battery-electric trains is seldom straightforward and requires careful analysis. This design problem is especially challenging for trains intended for use on routes involving significant distances, few intermediate stations and prolonged steep gradients. The work being reported here involves more detailed modelling of on-board power transmission systems and describes the application of model-based analysis methods and simulation techniques to estimate fuel cell and battery power ratings and battery storage capacity. The case considered here involves a three-coach hybrid configuration and differs significantly from that discussed in the previous report in a number of ways.

Conventional simulation methods applied to train performance investigations allow estimates to be made of variables such as speed or position, usually as functions of time, for inputs such as tractive force or power. However, an inverse simulation approach is adopted here which provides the tractive force or power at the rail for a given time history of distance travelled as input. This allows direct investigation of power ratings and storage capacity for the fuel-cell stack and battery pack for specified levels of train performance defined by a required schedule.

The mathematical model of the train, on which the simulation is based, is considered in two parts. The standard equations describing longitudinal train movement form the first part of the model, with the equations describing the hydrogen fuel-cell stack, battery pack, power electronic components and traction motors forming a separate sub-model. A simple test route is used initially, with several distinct stages. These involve acceleration from rest, steady state running at the line speed limit, a section with a steep rising gradient and subsequent stages involving coasting and braking. From the analysis carried out using this model and the simulation results from the test route, estimates are made of power and stored energy requirements for a specific section of the West Highland line.

From the results it is suggested that a specification for a three-coach hybrid unit for use on steeply graded secondary routes could be based on three 250 kW traction motors, a fuel-cell stack providing a maximum power output of 500 kW together with a 375 kW battery pack providing between 210 kWh and 300 kWh of storage. Preliminary weight estimates suggest that this specification could be achieved for a three-coach train for a gross weight of the order of 135 tonnes, although the volume of the necessary equipment could (at the present time) be difficult to accommodate within restrictions imposed by the UK loading gauge. These calculations allow for inclusion of a pantograph and associated equipment for operation from 25 kV supplies on electrified routes.

Conclusions are also reached about additional insight provided by the inverse simulation approach compared with conventional simulation methods when applied to powertrain design issues. It is believed that these benefits could apply also to investigations involving other forms of on-board power transmission and energy storage systems

**Keywords:** Inverse; simulation; train performance; hydrogen fuel cell; battery; powertrain.

# CONTENTS

## 1. Introduction

Hybrid powertrain systems involving hydrogen fuel cells in conjunction with batteries are attracting much attention in the context of rail network de-carbonisation, especially for secondary routes that lack the traffic density to justify conventional electrification [1]-[3]. In some cases, such as the West Highland lines from the central belt of Scotland to Oban and Fort William, these secondary routes involve relatively long distances and have sections involving severe gradients and few intermediate stations. Assessment of the potential of hydrogen-powered trains for routes of this kind in Scotland has recently been recognised as a priority by Transport Scotland [2]. The work being discussed here builds on and extends a report, prepared for the Scottish Association for Public Transport (SAPT) in June 2020, entitled *Modelling and simulation of hybrid electric trains powered by hydrogen fuel cells and batteries for routes in the highlands of Scotland*: *Preliminary results* [4]. That report outlines some issues arising in the design of powertrain systems for hybrid hydrogen fuel-cell/battery-electric trains and includes preliminary simulation results for the case of a two-coach multiple-unit train. A more general review of developments in electrical battery, fuel cell and energy recovery systems for railway applications was prepared for SAPT in November 2019 and that review includes additional background information [5].

Designs of hybrid powertrains incorporating fuel cells and energy storage components, such as batteries, cover a range of possible configurations. Some systems that have been proposed are essentially battery powered, with the fuel cell being used to provide battery charging and thus extend the range. Other proposed systems are powered mainly from the fuel cell, with the battery providing short-term storage of energy from regenerative braking. Previous studies involving multiple-unit trains with hybrid powertrains incorporating hydrogen fuel cells and batteries, have been concerned mainly with routes involving frequent stops and only short sections with gradients of any significance [6], [7]. The application considered here relates to multiple-unit passenger train services for rural routes with distances between stops of the order of 12 km, or more, and lengthy sections involving gradients which may be as steep as 1 in 50 (2%) for considerable distances. Broader issues concerning the infrastructure required for hydrogen supplies and location of re-fuelling systems have not been considered in this paper and discussion of these topics can be found elsewhere (e.g. [1]-[3], [7]). Operating costs of trains involving hydrogen fuel cells is another topic which has not been considered as this is highly dependent on the costs of hydrogen production. As pointed out previously [3], hydrogen power is most attractive in parts of the country where hydrogen can be produced at low cost from renewable energy sources and where there are opportunities to support integrated rail, bus and other transport applications using this fuel. Hydrogen might therefore be best used in remote areas with inexpensive renewables where transmission links to the national grid are limited in their capacity [3], [5].

In addition to the fact that fuel cells are not reversible, the variation of fuel cell efficiency with operating condition and their sluggish dynamic response to demanded changes of output power level are important issues. Batteries also introduce system design problems since, to prolong their useful life, it is desirable to ensure that stored energy levels do not drop to low levels. Common practice involves operation in a range between about 30 and 85% of full battery charge and some have recommended that at least 50% of the peak charge level should be maintained [6].

Figure 1 shows a block diagram of the powertrain configuration considered. In this, the fuel cell stack is the primary source of energy and is assumed to be in an optimum steady state for most operating conditions, thus avoiding dynamic response issues. Energy stored in the battery pack augments the fuel cell power output when the train is accelerating or operating on an adverse gradient and the batteries can be re-charged during periods of regenerative braking. When the full fuel cell power output is not required for traction, such as when the train is coasting or stationary, the batteries are charged from the fuel cell stack.

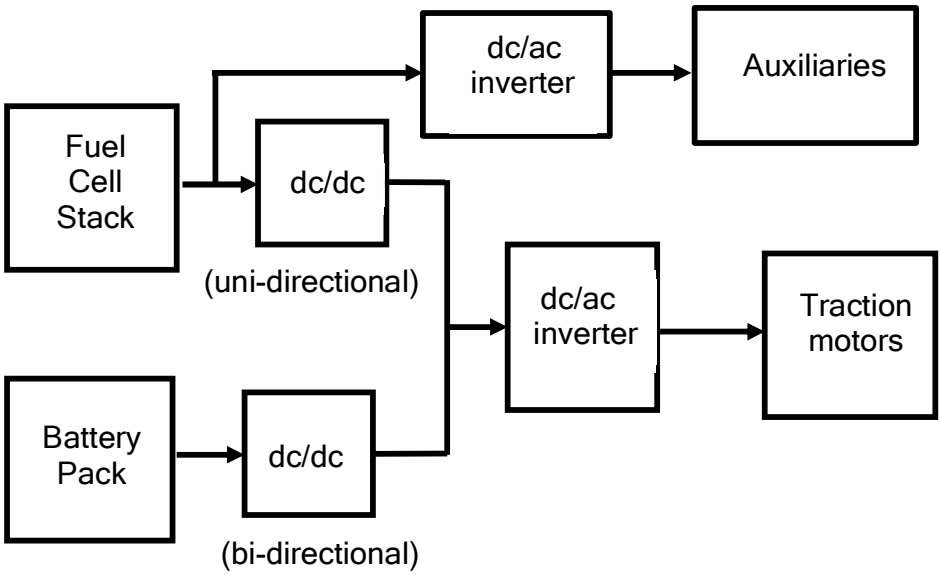


**Figure 1**. Block diagram of a hybrid powertrain system with fuel cell stack and battery pack coupled to traction motors through dc/dc converters and an inverter. Auxiliaries are supplied from the fuel-cell stack through a separate inverter.

Computer simulation methods used for train performance investigations normally apply tractive force or power as input variables and generate a distance versus time record as output, for given train parameters and route characteristics. In the inverse simulation approach [8] a desired schedule is used as input and time histories of tractive force or power at the rail are found as outputs.

The inverse approach to simulation has been used extensively in some other areas of engineering, such as aerospace systems [9] and automotive vehicle transmission design [10]. Benefits found in those applications, when compared with conventional forward simulation methods, include greater design insight and more direct investigation of design trade-offs. Previous work on inverse simulation applied to train performance issues has shown that this approach allows direct assessment of the effect of train parameters on the power and energy requirements in meeting a given schedule [11]. The effects of variations of journey time, changes in route characteristics or the choice of braking strategy can also be examined more directly using the inverse approach. The aim of this paper is to apply inverse simulation methods to the design of powertrains in hybrid rail vehicles and to consider benefits resulting from this approach.

## 2. Mathematical model development

The mathematical model of the train, on which the simulation work is based, is considered in two parts. The standard equations describing longitudinal train movement form the first part of the model, with the equations describing the hydrogen fuel-cell stack, battery pack, power electronic components and traction motors forming a separate sub-model. A simple test route is used initially, with several distinct stages. These involve acceleration from rest, steady state running at the line speed limit, a section with a steep rising gradient and subsequent stages involving coasting and braking.

### 2.1 The mathematical model for longitudinal train motion

In most mathematical models used in train-performance studies, the train is regarded as a single mass acted upon by the tractive force, braking force, gravitational forces associated with gradients and resistive forces (e.g. [11]-[13]). The distance travelled as a function of time, $x(t)$, is taken as an output quantity, along with the velocity $\dot{x}(t)$ and the acceleration $\ddot{x}(t)$. From the application of Newton's Second Law, the equation of motion has the form:

$$M(1+\phi)\ddot{x}(t) = F_T(t) - F_B(t) - R(t) \pm Mg\sin\alpha(x(t)) \tag{1}$$

where $F_T(t)$ and $F_B(t)$ are the tractive and braking forces, respectively. The variable $R(t)$ is the resistance to motion, $g$ is the acceleration due to gravity, $\alpha$ is the gradient angle of the track (which depends on $x(t)$) and $M$ is the gross mass of the train, which is regarded as constant. The factor $(1+\phi)$ is used to represent added mass associated with inertial effects due to rotating parts (e.g. [11], [12]).

The resistance $R(t)$ in equation (1) is described by the Davis equation (e.g. [11], [12], [14]) involving a polynomial in $\dot{x}(t)$ of the form:

$$R(t) = A + B\dot{x}(t) + C\dot{x}(t)^2 \tag{2}$$

Equation (2) neglects resistance due to track curvature and resistance effects in tunnels. If necessary, additional terms may be introduced to allow for these effects.

The terms $F_T(t)$ and $F_B(t)$ in equation (1) are linked so that when the tractive force term $F_T(t)$ has a non-zero value the braking force $F_B(t)$ is zero and vice versa. Together these terms form a composite tractive force variable $T(t)$ which can be positive or negative. The power at the rail, $P_R(t)$, is then given by the equation:

$$P_R(t) = T(t)\dot{x}(t) \tag{3}$$

Thus, for a specific value of power at the rail, the tractive force is inversely propoertional to the velocity However, for speed values below a specific transition value, $V_{ch}$, the available tractive force is limited to a value $T_0$ to ensure that adhesion between the driven wheels and the rails is maintained, even under adverse conditions. This transition speed is given by:

$$V_{ch} = \frac{P_{Rmax}}{T_0} \tag{4}$$

where $P_{Rmax}$ is the maximum value of power available at the rail. The energy consumption $E$ over the period from the start $t = 0$ to time $t = \tau$ is given by:

$$E = \int_0^\tau P_R(t)dt \tag{5}$$

In general, braking action may be frictional or may involve regenerative braking strategies based on a blend of frictional and electrical braking. With purely frictional braking it may be assumed that the driver employs a progressive strategy in which the braking force is inversely proportional to speed. The braking power may then be considered constant in the early stages of braking and, in the model used here, this is taken as equal to $P_{Rmax}$. In the second phase of a frictional braking strategy the braking force may be limited by adhesion and is taken to be equal to the tractive force value at the adhesion limit, $T_0$. With regenerative braking, the force is limited by the power ratings of the traction motors, electronic components and batteries. As the speed falls the braking force increases in accordance with equation (3) until it reaches the value $T_0$. The braking force then remains at that adhesion limit until the train comes to rest.

The form of model described by equations (1) – (5) has been applied widely for many purposes and has been subjected to extensive validation involving the use of data from measurements made during practical train performance tests (e.g. [12], [13], [15]).

### 2.2 The hybrid powertrain sub-model

The fuel-cell model involves an ideal energy source with a specified output power rating. Dynamic effects could be expected since fuel cells can take a significant time to respond to demanded changes of output power level. However, in this case, a simple energy management system ensures that the fuel cell stack and battery pack operate in a coordinated way so that the stack is in a steady state under almost all conditions of train operation.

Dynamic effects are also neglected in the highly simplified battery pack description that is used. A maximum power rating is specified for the charging process and a battery efficiency factor is included to allow for the fact that some energy is inevitably lost within the battery between charge and discharge. The power electronic blocks in Figure 1, are also modelled in a simplified way, with the output power of each inverter or dc/dc converter being taken as a fixed percentage of the input power (for power transfer in both directions in the case of the bi-directional units). Similarly, a highly simplified form of model is used to represent the traction motors, with the power at the rail being a fixed percentage of the power output at the traction motor inverter block in Figure 1.

In Figure 1 the dc/dc power electronic converter associated with the fuel cell is unidirectional, as the fuel cell cannot absorb electrical energy, but the dc/dc converter block connected to the battery is bi-directional, as is the main dc/ac inverter that supplies the traction motors. There is a block representing auxiliary services such as heating, air conditioning and all electrical services which are not associated with traction. It is assumed that this auxiliary load is supplied continuously by the fuel cell through a unidirectional inverter.

The power at the rail from the fuel cell is thus given by:

$$P_{RFC}(t) = \left( P_{FC}(t) - \frac{P_{AUX}}{\eta_{AUX}} \right) \eta_{DC1}\ \eta_{INV}\ \eta_M \tag{6}$$

where $P_{FC}(t)$ is the power output of the fuel cell, $P_{AUX}$ is the constant power required for auxiliaries, supplied through the inverter of efficiency $\eta_{AUX}$. The efficiency of the unidirectional dc/dc converter for the fuel cell is $\eta_{DC1}$ and the efficiencies of the inverter and traction motors are $\eta_{INV}$ and $\eta_M$ respectively.

If $T(t)$ is positive, the required power at the rail $P_R(t)$ is given by equation (3). If this exceeds the power available from the fuel cell, $P_{RFC}(t)$, additional power at the rail $P_{RB}(t)$ must be supplied by the battery as follows:

$$P_{RB}(t) = P_R(t) - P_{RFC}(t) = T(t)\dot{x}(t) - \left( P_{FC} - \frac{P_{AUX}}{\eta_{AUX}} \right) \eta_{DC1}\ \eta_{INV}\eta_M \tag{7}$$

This additional power at the rail is related to the battery power $P_B(t)$ through the equation:

$$P_{RB}(t) = \eta_{DC2}\eta_{INV}\eta_M P_B(t) \tag{8}$$

where $\eta_{DC2}$ is the efficiency of the bidirectional dc to dc converter.

Hence, from equations (7) and (8), the power drawn from the battery is given by:

$$P_B(t) = \left\{ \frac{T(t)\dot{x}(t)}{\eta_{DC2}\eta_{INV}\eta_M} - \left( P_{FC} - \frac{P_{AUX}}{\eta_{AUX}} \right) \frac{\eta_{DC1}}{\eta_{DC2}} \right\} \tag{9}$$

If $T(t)$ is positive but the required power at the rail, $P_R(t)$, is less than the power available from the fuel cell, part of the fuel cell output may be used for traction and part for recharging the battery. Losses that arise in the battery are accounted for through the factor $\eta_B$ which is the efficiency measure representing the percentage of charge power converted into usable stored energy. The useful power for battery charging (provided it is less than the specified maximum $P_{BMAX}$) is then given by:

$$P_B(t) = \left\{ \left( P_{FC} - \frac{P_{AUX}}{\eta_{AUX}} \right) \eta_{DC1}\ \eta_{INV}\eta_M - T(t)\dot{x}(t) \right\} \eta_B\eta_{DC2}\eta_{INV}\eta_M \tag{10}$$

During coasting, no power is drawn by the traction motors and power from the fuel cell is used for battery charging, giving:

$$P_B(t) = \eta_B\eta_{DC2} \left( P_{FC}(t) - \frac{P_{AUX}}{\eta_{AUX}} \right) \eta_{DC1} \tag{11}$$

During regenerative braking, the power for battery charging is limited to the maximum that the traction motor can provide in generator mode and by the maximum power that can handled by the battery itself, $P_{BMAX}$. Subject to those limits the effective power at the battery input, $P_B(t)$, during regenerative braking is given by:

$$P_B(t) = \eta_{DC2}\eta_{INV}\eta_M\eta_B T(t)\dot{x}(t) \tag{12}$$

The efficiency of the motors during regeneration is taken to be the same as the efficiency in normal operation.

Regenerative braking is used in the simulatin model until the train speed drops to the threshold value, $V_{ch}$, at which tractive effort limiting occurs. In the final stage of braking, frictional braking is used with negative tractive force applied equal to the adhesion limit, $T_0$ . During that phase, the battery is charged from the fuel cell through the dc/dc converters, in accordance with equation (11) and this also applies when the train is at rest. When the speed reaches zero the tractive force, braking force, resistance and gradient terms in the equation of motion (1) are set to zero to ensure that no further movement can occur.

The powertrain sub-model used involves a very simple form of energy management system, as implied by the description given above. The fuel-cell stack provides a constant power output except during regenerative braking when the power output from the fuel-cell stack is reduced to an idle level involving only the constant component for the auxiliaries

Note that, under steady state conditions, equation (9) can be written as:

$$P_B = -\frac{\eta_{DC1}}{\eta_{DC2}} P_{FC} + \frac{1}{\eta_{DC}\ \eta_{INV}\eta_M} P_R + \frac{\eta_{DC1}}{\eta_{DC2}}\left(\frac{P_{AUX}}{\eta_{AUX}}\right) \tag{13}$$

This is the equation of a straight line which allows the battery power $P_B$ to be defined for a given fuel cell power rating $P_{FC}$ and a specific power at the rail $P_R$. For the parameter values given in Table 1 this straight line relationship has the form:

$$P_B = -P_{FC} + 1.11P_R + 153.84 \tag{14}$$

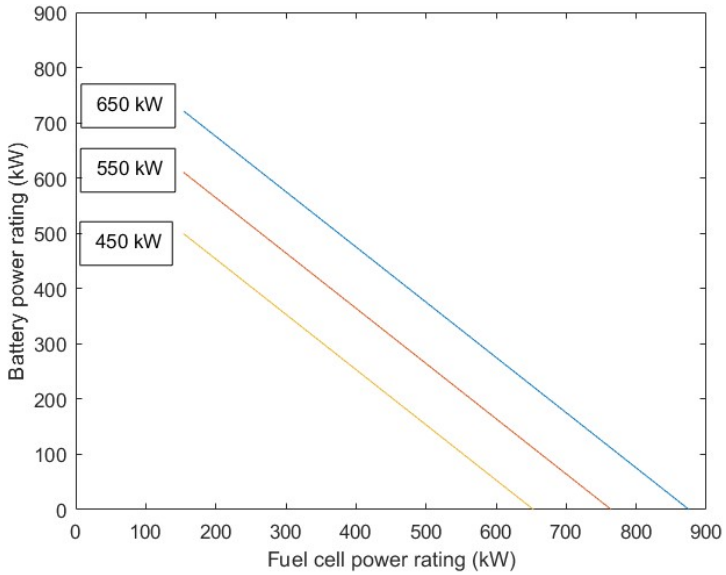


**Figure 2.** Relationship between battery and fuel cell power for three values of steady-state power at the rail (650 kW, 550 kW and 450 kW).

Figure 2 show this linear relationship for three power values. An approximate steady-state situation, such as during the initial acceleration or travel over a section of line involving a constant rising gradient, could provide a relevant steady power value. For example, if the required power at the rail is 550 kW it is clear from equation (14) and Figure 2 that the minimum fuel-cell power rating is 153.84 kW which is sufficient only to provide the power for auxiliaries, whereas the maximum is approximately 764 kW, corresponding to the case where there is no battery.

**Table 1:** Parameter values used in initial simulation runs for the three-coach hybrid fuel-cell and battery-electric unit (e.g. [6], [7]).

| Quantity | Symbol | Numerical value, with units |
|---|---|---|
| Traction motor power rating | $P_M$ | 750 kW |
| Hydrogen fuel-cell stack power rating | $P_{FC}$ | 500 kW |
| Train mass (gross) | $M$ | 130,000 kg (130 tonnes) |
| Rotational mass term | $\Phi$ | 0.08 |
| Tractive force at zero speed | $T_0$ | 50 kN |
| Traction motor efficiency | $\eta_M$ | 0.95 |
| DC/DC converter efficiencies | $\eta_{DC1}, \eta_{DC2}$ | 0.975 |
| Inverter efficiencies | $\eta_{INV}, \eta_{AUX}$ | 0.975 |
| Battery efficiency | $\eta_B$ | 0.85 |
| Maximum battery power (chargng) | $P_{Bmax}$ | 346 kW |
| First resistance coefficient | $a$ | 1500 N |
| Second resistance coefficient. | $b$ | 6.0 $Nm^{-1}s$ |
| Third resistance coefficient | $c$ | 6.7 $Nm^{-2}s^2$ |
| Gravitational constant | $g$ | 9.81 $ms^{-2}$ |
| Power for auxiliaries | $P_{AUX}$ | 150 kW |

The power ratings of the traction motors and fuel-cell stack and the storage capacity and power rating of the battery pack have an important influence on the overall mass of the train. Using published information [6], [7] it is possible to make a first estimate of the mass of the powertrain components. For example, in order to provide an overall power output of 500 kW from the fuel-cell stack, five fuel cells would be needed giving a total fuel-cell mass of about 2.5 tonnes when account is taken of associated equipment (such as the coolant pump, air blower and dc/dc converter). A typical 22 kWh battery has a mass of 650 kg so that a specification involving a storage capacity of 150 kWh and power rating of about 350 kW would require a pack involving at least seven batteries, giving a mass of 4.55 tonnes. Typical traction motors with the rating considered have a mass of about 600 kg each, giving a total motor mass of 1.8 tonnes. Other electrical equipment, such as the power electronic inverters and dc/dc converters, could add about 1.7 tonnes to the basic mass of the train while hydrogen storage tanks, pipework and a compressor would represent a further 1.8 tonnes [7]. The estimated total mass for the powertrain is therefore about 12.4 tonnes, with a further 4 tonnes to be added for the addition of a pantograph with associated circuit breakers and transformer [7]. Thus, the total mass of the powertrain and traction equipement is approximately 16.4 tonnes. An estimate of the basic mass of each coach is 31 tonnes, so that the tare mass of a fully-equipped three coach fuel-cell/battery-electric multiple-unit train would be 112.4 tonnes. Using a factor of 1.08 for added mass due to inertial effects, the effective tare mass is of the order of 121.4 tonnes and, allowing an additional 9 tonnes for passengers and luggage, the first estimate of the gross mass is 130.4 tonnes.

The value shown in Table 1 of 135 tonnes has been chosen to allow for possible changes in fuel-cell and battery ratings suggested by results found from this investigation .

### 2.3 Modelling of the route and driver control actions

A section of route has been defined for the simulation, with features typical of lines on which hybrid hydrogen fuel-cell/battery-electric trains might operate. The length of the test route is approximately 15 km and involves five distinct phases of operation: a) the initial phase on level track involving acceleration to the maximum allowed line speed, b) a steady-state phase of continuous operation within the line-speed limit but with a significant change of gradient over part of that section, c) a phase involving a further section of level track, d) a coasting phase and e) a final braking phase to bring the train to rest. In the example being considered the coasting phase begins at a distance of about 11.3 km from the start and the braking phase at a distance of about 14.3 km.

The chosen gradient profile involves level track for an initial distance of 4 km and then a constant rising gradient of 1 in $Y$ for 4 km, with a value of $Y$ of 60 chosen for this study. The angle $\alpha$ in equation (1) is related to $Y$ through the equation:

$$\sin \alpha = 1/Y \tag{15}$$

Practical train performance simulation models should allow for speed restrictions and provide smooth transitions to speed-limited sections of route. The model therefore includes a simplified representation of driver action in which speed is compared continuously with the speed limit for the current position of the train and, as in previous work, the tractive force value at each time step in the simulation is multiplied by a factor $C_{ds}(t)$ to represent driver control actions in approaching and adhering to the speed limit [11]. Control actions associated the start and end of coasting and the initiation of braking, are incorporated into the route model.

## 3. Computational methods

Computational tools, such as MATLAB® [16] or the broadly-similar open-source Scilab software [17] are useful for the simulation of.systems described mathematically by a combination of ordinary differential equations and algebraic equations. These software tools are based on well-established numerical techniques and are therefore robust, well-documented and highly relevant for studies of train performance.

The simulation programs developed for this work are written in MATLAB® code, using standard '*ode*' routines for solution of the ordinary differential equations. Several different *ode* routines are available within MATLAB® but the all results presented here are based on the use of the low-order *ode23* routine involving a Runge-Kutta algorithm.

### 3.1 The inverse simulation approach

Several methods of inverse simulation have been developed (see e.g. [8]-[11]) and these can be implemented using standard tools such as MATLAB®. The specific method used in this work is described in detail elsewhere (e.g. [11], [18], [19]) and involves the application of a high-gain feedback path around a conventional train performance simulation model, as shown in Figure 3. The main feedback loop involves the difference between a desired time history distance record, $x_{ref}(t)$

and the corresponding distance, $x(t)$, obtained from the simulation. A secondary feedback pathway involving the speed $\dot{x}(t)$ provides damping of high frequency oscillatory transients that can be an undesirable feature of high-gain feedback systems. Such velocity feedback compensation is widely used in the design of feedback systems for automatic control applications. The complete feedback equation thus has the form:

$$T(t) = K_1\left(x_{ref}(t) - x(t)\right) - K_2\,\dot{x}(t) \tag{16}$$

where the variable $T(t)$ is the tractive force needed to match the given input data set $x_{ref}(t)$. The distance-error gain factor $K_1$ and the velocity-feedback gain factor $K_2$ have been chosen on a trial and error basis, guided by experience from other applications of inverse simulation. In this case values of $10^8$ and $1.5\times10^4$ have proved satisfactory for $K_1$ and $K_2$, respectively.

The reference input used in this investigation is derived from a model of an existing train to ensure that the schedule defined by the reference input is realistic in terms of the longitudinal dynamics and does not impose unrealistic and physically implausible demands. The train chosen as reference for this investigation is a three-coach Class 159/1 diesel multiple unit (dmu) which has 90 mph capability and is used in the United Kingdom on some mainline and secondary routes. A mathematical model has been developed for this class of unit which involves the basic features of the train model described by equations (1)-(5), together with a simple representation of the diesel engines and transmission system. Parameter values are given in Table A1 in the Appendix and representation of the route and driver control actions for this reference model are as described in the sections above.

The variable $x_{ref}(t)$, which provides the reference input in equation (16), is generated from a forward simulation for the dmu and values for the power at the rail found from this forward simulation also provide a first estimate of power ratings for the fuel-cell stack and battery pack, using equation (14). For example, the forward simulation results show that the maximum power at the rail for the dmu is 644 kW, occurring during the initial acceleration. With a fuel cell power rating of 500 kW (as in Table 1), equation (14) shows that the battery power rating must be at least 369 kW. Also, from the information above, it is clear that the traction motor power rating to match the dmu performance must be at least 644 kW. A slightly larger value (750kW) has been used in Table 1 to allow for possible journey-time improvements. Although the above analysis provides a possible first estimate of the power rating of the battery, it does not provide information about the stored energy requirements. Fuel-cell and battery power ratings and requirements in terms of stored energy capacity must be investigated more fully using the inverse simulation model.

As shown in Figure 3, the primary output variable of the inverse model is the tractive force, $T(t)$. Other variables obtained from the inverse model, include the distance travelled, $x(t)$, and the speed, $\dot{x}(t)$, with the core block of the inverse model being based on equations (1) and (2). From knowledge of $T(t)$ and $\dot{x}(t)$ additional variables, such as $P_R(t)$ and $P_B(t)$ may then be derived using equations (3)-(12). The inverse model does not include speed limits or driver actions explicitly since by matching the given reference input, $x_{ref}(t)$, this inverse model automatically satisfies these constraints.

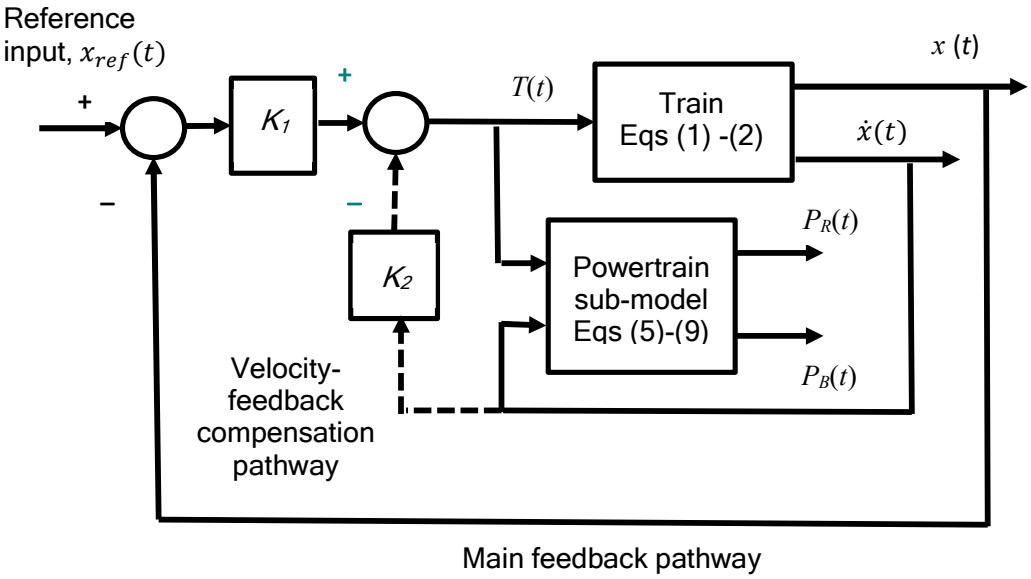


**Figure 3.** Block diagram illustrating the high-gain feedback approach to inverse simulation as applied to the model of the hybrid fuel-cell/battery-electric multiple unit. The inverse simulation model is the complete closed-loop system including the train and powertrain model blocks. The reference input is the desired distance/time record, while the primary output variable of the inverse model is the tractive force, $T(t)$.

## 4. Investigation of fuel cell and battery ratings through inverse simulation

Figure 4 shows a typical distance versus time data record generated from the simulation model for the Class 159/1 dmu for the parameter set of Table A1 and the standard test route described previously. This forms the reference input $x_{ref}(t)$ used in the inverse simulation. The main feedback pathway of Figure 3 forces the inverse simulation model to follow the reference input, thus defining the required schedule in terms of the distance travelled and journey time. In that high gain feedback loop the difference between the reference, $x_{ref}(t)$ and the corresponding inverse simulation variable, $x(t)$, is very small, with values less than 0.01 m at all time instants over the complete record for the gain factors used.. Information from Figure 4 and the corresponding speed versus time record in Figure 5 shows very clearly the five distinct phases of operation over the test route. It can be seen from these simulation records that he train comes to a halt after 665 s, approximately 15.1 km from the starting point and that the 96 km/h line speed limit is adhered to.

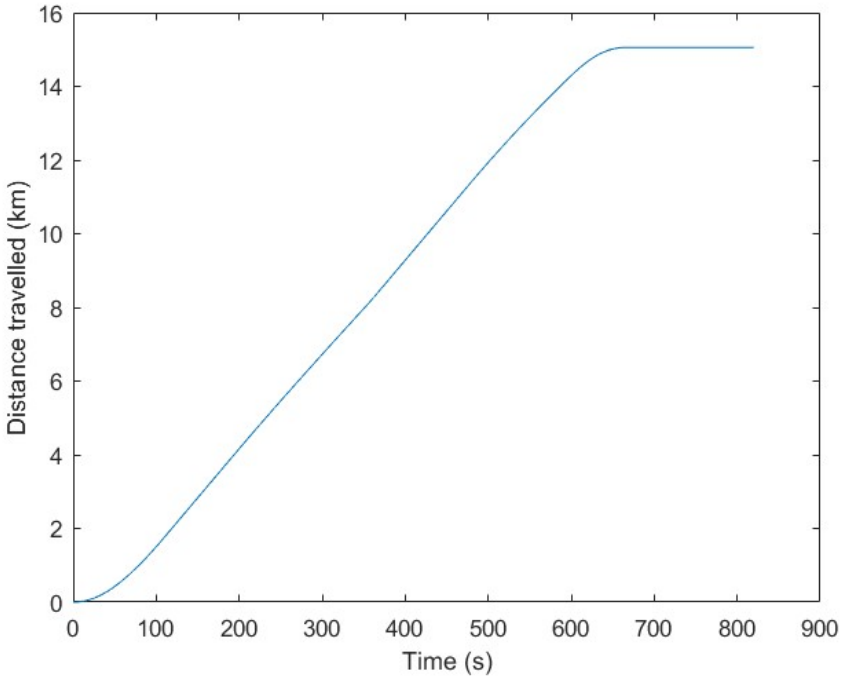


**Figure 4.** Distance versus time record used as reference input for the inverse simulation.

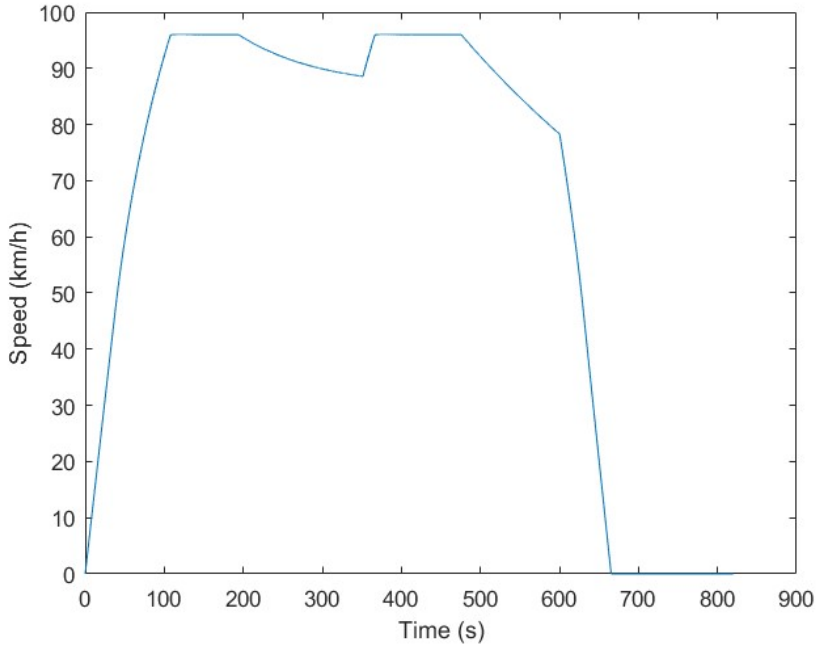


**Figure 5.** Speed versus time record from the inverse simulation of the hybrid fuel-cell and battery-electric unit for the parameters of Table 1 and the reference input of Figure 4.

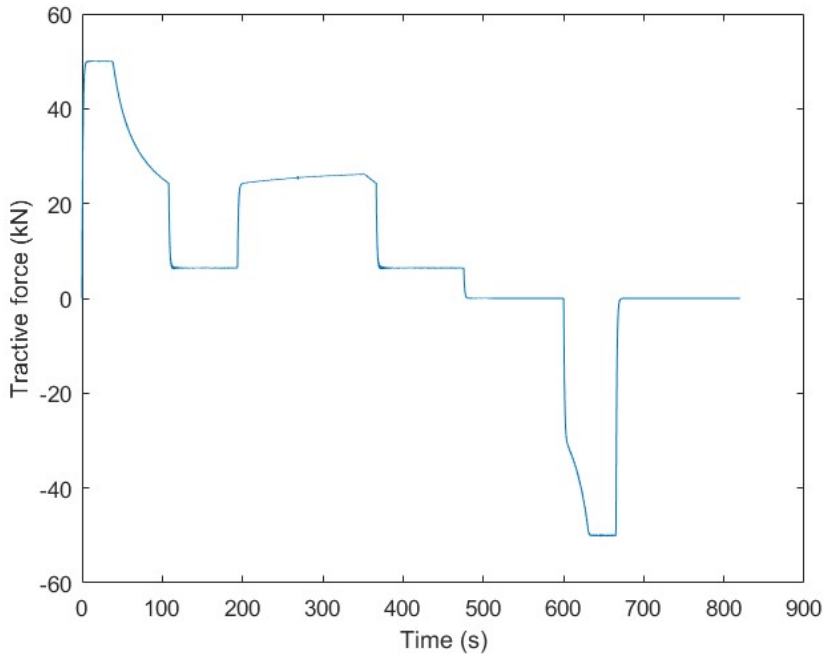


**Figure 6.** Tractive force time history from the inverse simulation for the reference input of Figure 4.

Figures 6 and 7 show the tractive force time history and power at the rail, respectively, with negative values indicating braking action. The tractive force variable is the primary output of the inverse simulation and Figure 6 shows that its time history is influenced, very strongly, by the route characteristics. It is limited initially by adhesion before reaching the constant-power condition at a speed of about 12 m/s. The corresponding value of power at the rail is then approximately 645 kW. At speeds greater than this a constant power condition applies and tractive force falls as the speed increases (as in equation (3)). When the speed reaches the line limit of 96 km/h the tractive force and power levels fall to values well below half the maxima seen during the initial accceleration. The start of the rising gradient shows increases in tractive force and power at the rail. The train accelerates on the level track beyond the summit until the line speed limit is reached and this is followed by periods of coasting and then regenerative braking. When the speed drops below 12 m/s, frictional braking is used with a negative tractive force equal to the 50 kN adhesion limit.

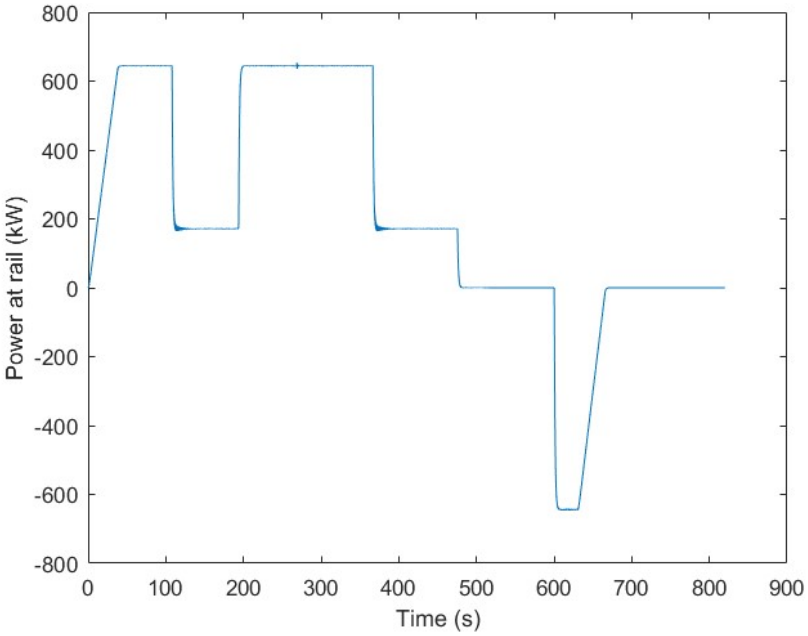


**Figure 7.** Power at the rail time history from the inverse simulation for the reference input of Figure 4.

Figure 8 shows the battery power levels during the journey, with negative values of battery power indicating that battery energy is being supplied for traction, while positive values show that battery charging is taking place. The largest values of battery power supplied for traction (about 366 kW) occur during the part of the acceleration phase when the tractive force is not limited by adhesion and also during the gradient ascent. During all the periods when the battery is being charged directly from the fuel cell the maximum battery power has a value equal to the fuel cell power, after allowance is made for the auxiliary load, the efficiencies of the dc/dc converters, the battery charging power limit and battery losses accounted for by the battery efficiency factor. During regenerative braking the maximum battery charging power is determined by the braking power at the rail, the efficiency of the traction motors (when operating as generators), the inverter efficiency, the efficiency of the dc/dc converter associated with the battery, the battery efficiency factor and the battery power limit when charging.

Close examination of the tractive force and battery power time histories shows the presence of short transient bursts of high frequency oscillations at two points on the record (at about 100 s and at about 380 s). As mentioned previously, the two gain factors in the feedback loops are chosen to minimise such effects while providing the necessary accuracy in the inverse simulation and avoiding excessive computation times for simulation runs.

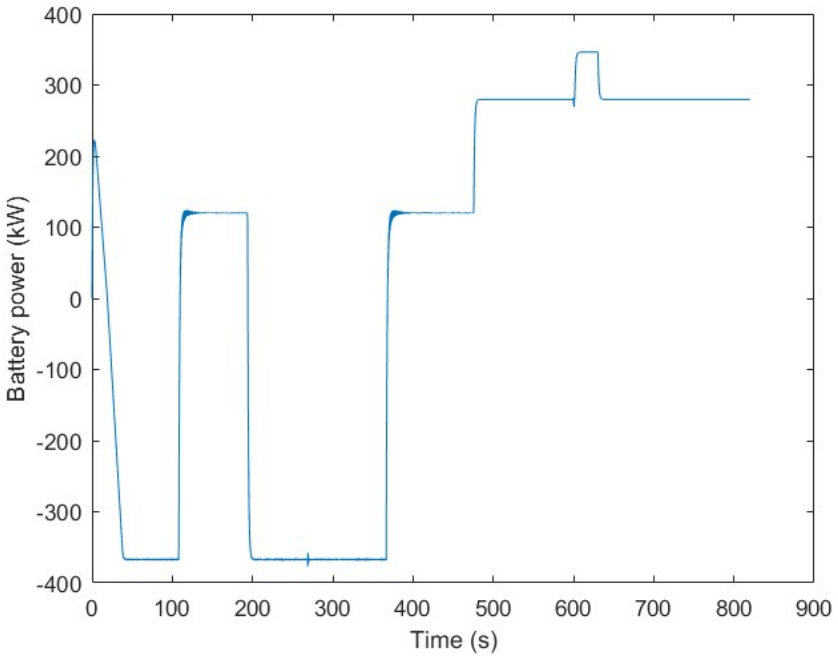


**Figure 8.** Record of battery power versus time from inverse simulation for reference input of Figure 7.

Figure 9 shows the variation of battery stored energy with time, for an initial condition of 100 kWh. The slope of this record during discharge and charge periods is important and determines the storage capacity needed for the intended application. For the train parameters and route used in this simulation study, the stored energy is seen to fall to a minimum of about 77 kWh and then to rise again in a vee shaped pattern during the periods when the train is coasting, braking and stationary. Since the battery power being supplied to the traction motors reaches a maximum of about 366 kW during the initial acceleration and during the ascent of the 1 in 60 gradient, the rate of change of stored energy during discharge is greatest during these two periods and has a value of about -6.1 kWh/min. The results show that, at 755 s from the start and following a ninety-second station stop, the battery charge has been restored to a level above the initial value due to charging while the train was coasting, braking and at rest, with an average charge rate of about 4.9 kWh/min.

An increase in the power rating of the fuel cell reduces the energy required from the battery, as suggested in Figure 2. For example, inverse simulation shows that a 600 kW fuel cell stack gives a reduction in traction power from the battery of almost 100 kW compared with the 500 kW case. The corresponding rate of change of battery stored energy is found to be -4.5 kWh/min compared with -6.1 kWh/min. Also, with the 600 kW fuel cell, the battery charges more rapidly during coasting, braking and when the train is stationary, with an average charge rate over those phases of operation of over 6 kWh/min. At 755 s, after the station stop, the stored energy level recovers to about 125 kWh, which is well above the initial condition of 100 kWh. This suggests that a trade-off between fuel cell power rating, battery power rating and battery stored energy requirements is possible. Finding a satisfactory combination is important since the overall train weight, the volume of powertrain hardware and the weight and volume of hydrogen storage required for a specific type of route are all affected directly by these ratings.

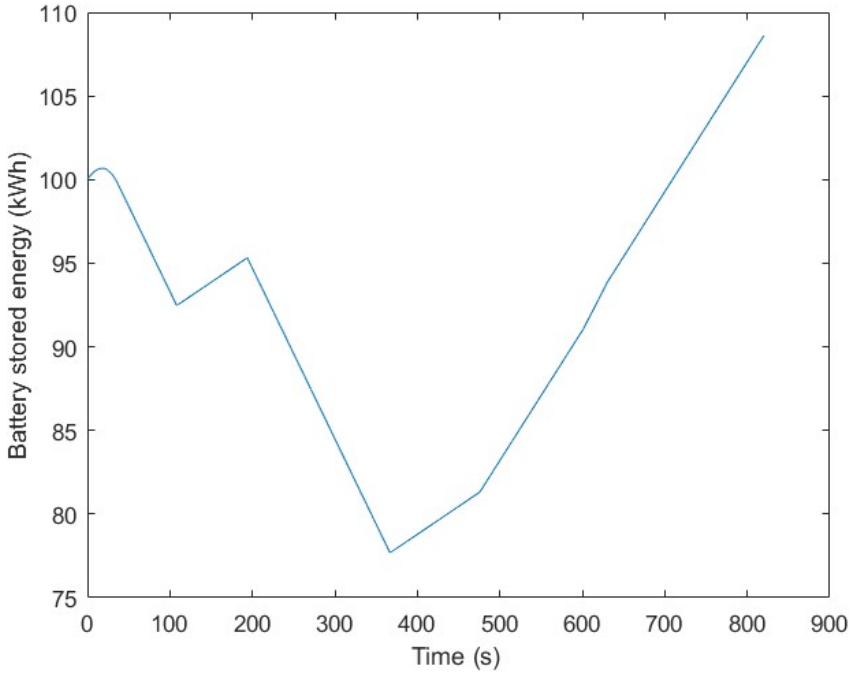


**Figure 9.** Battery stored energy versus time from inverse simulation of the hybrid multiple unit, for parameter value given in Table 1, for the reference input of Figure 4.

Inverse simulation allows us not only to investigate the effect of varying the fuel cell power rating on the required battery power and storage capacity needed to meet the schedule defined by $x_{ref}(t)$ but also allows direct investigation of the sensitivity of the results to variation of other train parameters, such as the mass or resistance characteristics. For example, it can be shown from inverse simulation that a reduction in the effective mass of the train by 15 tonnes reduces the maximum power drawn from the battery during the initial acceleration by about 25 kW. The inverse simulation approach is particularly useful for these parameter sensitivity investigations as comparisons are all made for the same required schedule, as defined by the reference input.

Inverse simulation methods also allow direct examination of the effects of varying the time required for the journey. The reference input can be adjusted using time scaling techniques that were developed first on analogue and hybrid computers (see e.g. [20]) This involves introducing an additional gain factor for each integration operation. For example, a factor of 1.05 associated with each integrator in a simulation model reduces the simulated time for that model by 5% and, similarly, a factor of 0.95 increases the simulated time by the same percentage.

Figure 10 shows the speed versus time record found through inverse simulation for a journey time reduction of 5%. Because the coasting and braking phases are defined by distances, they start at different times from those shown in Figure 5. However, the reduced journey time of just over 10½ minutes for the 15 km distance requires the maximum speed to exceed the line limit of 96 km/h. In matching the new reference schedule, the results also show an increase in the maximum power at the rail of about 95 kW and give an initial tractive force that is greater than the assumed adhesion limit. The overall stored energy costs for this reduced journey time have also increased, with the stored

energy level after the 90s station stop being 97.9 kWh compared with the corresponding value of 103.1 kWh for the original schedule.

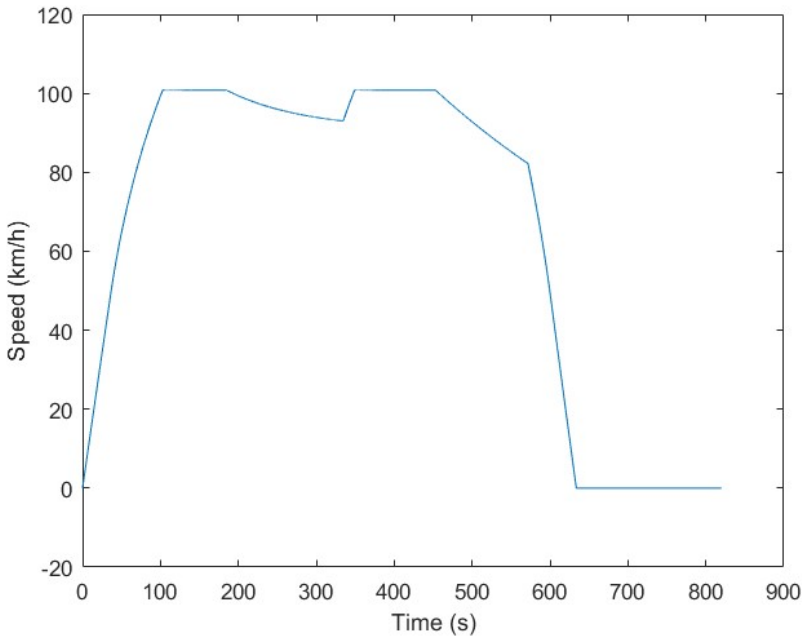


**Figure 10.** Speed versus time record from the inverse simulation of the hybrid multiple unit for the parameters of Table 1 and distance versus time reference input with all time values reduced by 5% .

## 5. Discussion

Extrapolation from the inverse simulation results for the test route allows estimates to be found for the powertrain characteristics needed for a specified schedule for a particular section of railway line. As mentioned in the introduction, the West Highland line in Scotland has long sections involving rising gradients where battery power could augment the energy from the fuel-cell stack and also long descents where the battery could be charged through regenerative braking or directly from the fuel cells while coasting. One typical situation involves the 29.6 km climb from Spean Bridge station to Roy Bridge, Tulloch and Corrour. The rising gradients vary, involving long sections at 1 in 59, 1 in 67 and at 1 in 57, before a summit is passed about ½ km before Corrour station. Current timings for diesel units on this section are, typically, 6 minutes from Spean Bridge to Roy Bridge, a further 10 minutes to Tulloch and then 16 minutes to Corrour. The simulation results for the test route involving the 1 in 60 rising gradient suggest that with three 250 kW traction motors, a hydrogen fuel-cell stack of 500 kW output and a battery pack providing a maximum power output of 375 kW, the level of battery stored energy would change at a rate of about -6.1 kWh/minute during the climb. The simulation results also suggest that stored energy could be recovered at an average rate of 4.9 kWh/minute during coasting, braking and stops, assuming station dwell times of of 1½ minutes. Thus, the estimated stored energy cost for the 29.6 km and 32 minutes of travelling time between Spean Bridge and Corrour is about 150 kWh. This figure allows for 3 minutes of dwell time, 5 minutes of coasting or braking, the additional energy costs of acceleration after each station and the fact that the average gradient is less steep than the 1 in 60 of the simulation test route.

The simulation does not take account of local speed restrictions or increased resistance on curved track, both of which would increase demands on the battery pack on uphill sections of the route. Thus, to ensure that the stored energy in the battery pack does not fall below 30% of the maximum capacity, the pack should have a capacity of at least 210 kWh (for a fuel-cell power rating of 500 kW and battery power rating of 375 kW). If the minimum stored energy were to remain above the 50% level, the rated storage capacity would need to be at least 300 kWh.

Using standard powertrain components (e.g. [6], [7]), approximate calculations suggest that a design based around the figures above could be implemented within a gross weight of approximately 135 tonnes for a three-coach unit. However, the limitations of the UK loading gauge could present difficulties in terms of accommodating the system within the available space. Implementation might only be possible, at the present time, at the cost of some passenger accommodation.

Although written as a report which is intended to be self-contained, the information presented here is closely linked to preliminary simulation work presented in an earlier report [4] and to a more wide-reaching review [5], both of which were prepared for members of the Scottish Association for Public Transport.

## 6. Conclusions

Extrapolation from inverse simulation results using a simplified model and test route can provide useful insight in considering design options for hybrid rail vehicles involving fuel-cell stacks and battery packs. Simulation results suggest that a specification for a three-coach hybrid unit for use on steeply graded secondary routes could be based on three 250 kW traction motors, a fuel-cell stack providing a maximum power output of 500 kW together with a 375 kW battery pack providing between 210 kWh and 300 kWh of storage. Weight calculations allow for inclusion of a pantograph and associated equipment for operation from 25 kV supplies on electrified routes.

Although useful information about the mass and volume of fuel-cell stacks and battery packs suitable for rail applications is available [6], [7] such figures rapidly become out of date as new developments take place. Current research and development activities are showing steady improvements in specific (gravimetric) and volumetric energy densities of batteries. Similarly, developments in fuel-cell technology, on-board hydrogen storage systems, traction motors and power electronics provide new opportunities for innovative design. Meeting the specification outlined above, without serious weight and volume difficulties, might thus become easier in the not too distant future

In conclusion, the inverse simulation approach provides benefits in the investigation of traction system performance since it allows different configurations to be compared for a specified distance and journey time in every case. This avoids iterative procedures that would be necessary when applying conventional simulation methods. The approach could also be useful in addressing design issues in other hybrid powertrain configurations where battery packs, supercapacitors or flywheel energy storage systems are used to supplement hydrogen fuel cells or conventional electrical drives.

**Acknowledgements**

I wish to thank members of the Scottish Association for Public Transport and others, including some in the rail industry, for their feedback following the publication of the earlier reports on hybrid electric trains powered by fuel cells and batteries [4], [5]. Their comments and questions have proved helpful in the preparation of this paper.

**References**


1. RSSB. *Options for traction energy decarbonisation in rail: final report (T1145 Report)*. RSSB, UK. 12 June 2019. www.catalogues.rssb.co.uk . (Accessed 8 August 2020).

2. Transport Scotland. *Rail services decarbonisation action plan.*28 July 2020. Transport Scotland, UK. www.transport.gov.scot . (Accessed 8 August 2020).

3. Shirres D and Baxter J. *The future of hydrogen trains in the UK.* Report, Institution of Mechanical Engineers, London, UK. https://www.imeche.org/docs/default-source/1-oscar/reports-policy-statements-and-documents/imeche-hydrogen-trains.pdf?sfvrsn=2 (2019, accessed 18 August 2020).

4. Murray-Smith DJ. *Modelling and simulation of hybrid electric trains powered by hydrogen fuel cells and batteries for routes in the highlands of Scotland: Preliminary results.* Technical report for the Scottish Association for Public Transport, 27 June 2020. http://eprints.gla.ac.uk/219364/1/219364.pdf (Accessed 8 August 2020).

5. Murray-Smith DJ *A review of developments in electrical battery, fuel cell and energy recovery systems for railway applications.* Technical report for the Scottish Association for Public Transport, 30 November 2019. http://eprints.gla.ac.uk/204435/1/204435.pdf (Accessed 8 August 2020).

6. Hoffrichter A, Hillmansen S and Roberts C. Conceptual propulsion system design for a hydrogen-powered regional train. *IET Electrical Systems in Transportation*. 2016; 6(2): 56-66.

7. Kent S, Gunawardana D, Chicken T and Ellis R (2016). *Future Railway Powertrain Challenge: Fuel Cell Electric Multiple Unit (FCEMU) Project. FCEMU Project-Phase 1 Report-Issue 1.* University of Birmingham, Hitachi Rail, Fuel Cell Systems Ltd., www.birmingham.ac.uk/Documents/college-eps/railway/1-Class-156-Fuel-Cell-Electric-Multiple-Unit-Feasibility-Study-Issue-1.pdf (2016, accessed 18 August 2020).

8. Murray-Smith DJ. The inverse simulation approach: A focussed review of methods and applications. *Mathematics and Computers in Simulation.* 2000; 53(4-6): 239-247.

9. Thomson DG and Bradley R. The principles and practical applications of helicopter inverse simulation. *Simulation Practice and Theory.* 1998; 6: 47-70.

10. Fröberg A and Nielsen L. Efficient drive cycle simulation. *IEEE Transactions on Vehicular Technology.* 2008; 57(3): 1442-1453.

11. Murray-Smith DJ. Development of an inverse simulation method for the analysis of train performance, *Proc IMechE Part F: J Rail and Rapid Transit.* 2018; 232(5): 1295–1308.

12. Lukaszewicz P. *Energy consumption and running time for trains: modelling of running resistance and driver behaviour based on full scale testing.* PhD Thesis, Royal Institute of Technology, Stockholm, Sweden, 2001. https://pdfs.semantischolar.org/b2a1/478bb878493fb4eee06e89f847d649309.pdf. (Accessed 8 August 2020).

13. Douglas H, Weston P, Kirkwood D, Hillmansen S and Roberts C. Method for validating the train motion equations used for passenger rail vehicle simulation, *Proc IMechE Part F: J Rail and Rapid Transit.* 2017; 231(4): 455-469.

14. Davis WJ Jr. The tractive resistance of electric locomotives and cars. *General Electric Review.* 1926; 29: 685-707.

15. Salvador P, Martinez F, Villalbo, I and Insa, R. Modellling energy consumption in diesel multiple units *Proc IMechE Part F: J Rail and Rapid Transit* 2018; 232(5): 1539-1548.

16. Mathworks Inc. *MATLAB®/Simulink® modeling and simulation software.* http://www.mathworks.com/products/. (Accessed 8 August 2020).

17. Campbell SL, Chancelier J-P and Nikoukhah R. *Modeling and simulation in Scilab/Scicos.* New York: Springer, 2000.

18. Buchholz J and von Grünhagen W. *Inversion impossible?* Bremen: University of Applied Sciences, Technical Report, 2004.

19. Murray-Smith DJ. Feedback methods for inverse simulation of dynamic models for engineering system applications. *Mathematical and Computer Modelling of Dynamical Systems.* 2011; 17: 515-541.

20. Murray-Smith DJ. *Continuous system simulation.* London: Chapman and Hall, 1995, pp 216-217.

## Appendix

### Model of a Class 159/1 three-coach diesel multiple unit

A conventional forward simulation model of a three-coach Class 159/1 dmu provides the reference-input for the inverse simulation of the hybrid fuel-cell/battery-electric multiple unit. This is based on the train performance model described in the paper but with diesel engines and transmission systems replacing the hybrid powertrain sub-model. These are modelled in a highly simplified way, with a specified constant engine power and constant transmission efficiency under all operating conditions and with no dynamic effects included. The auxilary power load is assumed constant. Parameter values used for the Class 159/1 simulation are given in Table A1 below.

Braking is frictional with the applied force assumed, in the initial stage of braking, to be inversely proportional to train speed, giving a deceleration of 0.25m/s$^2$. This later increases to about 0.6 m/s$^2$ during the final stage when the braking force becomes equal to the tractive force value at the adhesion limit.

In addition to the distance time histories used as reference inputs for inverse simulation, this forward simulation of the dmu provides speed and other time histories for the specific input applied, including power at the rail information that provides a first estimate of power requirements for the hybrid multiple unit.

**Table A1**. Parameter values used in the simulation model for a Class 159/1 three-coach diesel multiple unit

| Quantity | Symbol | Numerical value with units |
|---|---|---|
| Engine power per 3-car unit, 3 Cummins 350 h.p. engines | $P_E$ | 783 kW |
| Train mass (gross) | $M$ | 130,000 kg (130 tonnes) |
| Rotational mass term | $\Phi$ | 0.08 |
| Tractive force at zero speed | $T_0$ | 50 kN |
| Transmission system efficiency | $\eta_{TRAN}$ | 0.88 |
| First resistance coefficient | $A$ | 1500 N |
| Second resistance coefficient | $B$ | 6.0 Nm$^{-1}$s |
| Third resistance coefficient | $C$ | 6.7 Nm$^{-2}$s$^2$ |
| Gravitational constant | $G$ | 9.81 ms$^{-2}$ |
| Power for auxiliaries | $P_{AUX}$ | 51 kW |